

Article

Synthesis and Characterization of Orange Peel Modified Hydrogels as Efficient Adsorbents for Methylene Blue (MB)

Saedah R. Al-Mhyawi ¹, Nader Abdel-Hamed Abdel-Tawab ² and Rasha M. El Nashar ^{2,*}¹ Department of Chemistry, College of Science, University of Jeddah, Jeddah 22233, Saudi Arabia² Chemistry Department, Faculty of Science, Cairo University, Giza 12613, Egypt

* Correspondence: rasha.elnashar@cu.edu.eg or rashaelnashar@gmail.com

Abstract: In recent years, due to the developments in the textile industry, water contaminated with synthetic dyes such as methylene blue (MB) has become an environmental threat based on the possible impacts in terms of chemical and biochemical demand, which leads to disturbance in aquatic plants photosynthesis, besides their possible toxicity and carcinogenicity for humans. In this work, an adsorbent hydrogel is prepared via free radical polymerization comprising acrylic acid (PAA) as a monomer and orange peel (OP) as a natural modifier rich in OH and COOH present in its cellulose and pectin content. The resulting hydrogels were optimized in terms of the content of OP and the number of cross-linkers and characterized morphologically using Scanning electron microscopy. Furthermore, BET analysis was used to follow the variation in the porosity and in terms of the surface area of the modified hydrogel. The adsorption behavior was found to follow pseudo-second-order as a kinetic model, and Langmuir, Freundlich, and Temkin isotherm models. The combination of OP and PAA has sharply enhanced the adsorption percent of the hydrogel to reach 84% at the first 10 min of incubation with an adsorption capacity of more than 1.93 gm/gm. Due to its low value of pHPZc, the desorption of MB was efficiently performed at pH 2 using HCl, and the desorbed OP-PAA were found to be reusable up to ten times without a decrease in their efficiency. Accordingly, OP-PAA hydrogel represents a promising efficient, cost-effective, and environmentally friendly adsorbent for MB as a model cationic dye that can be applied for the treatment of contaminated waters.

Keywords: adsorbent hydrogel; orange peel; methylene blue; poly acrylic acid hydrogel; cationic dyes

Citation: Al-Mhyawi, S.R.; Abdel-Tawab, N.A.-H.; El Nashar, R.M. Synthesis and Characterization of Orange Peel Modified Hydrogels as Efficient Adsorbents for Methylene Blue (MB). *Polymers* **2023**, *15*, 277. <https://doi.org/10.3390/polym15020277>

Academic Editor: Md Najib Alam

Received: 30 November 2022

Revised: 8 December 2022

Accepted: 8 December 2022

Published: 5 January 2023



Copyright: © 2023 by the authors. Licensee MDPI, Basel, Switzerland. This article is an open access article distributed under the terms and conditions of the Creative Commons Attribution (CC BY) license (<https://creativecommons.org/licenses/by/4.0/>).

1. Introduction

Clean water availability for drinking has been a highly important health challenge in recent years. Due to the rapid expansion in industrial effluents from the textile and petrochemical industries, environmental disturbances and pollution problems have highly emerged, affecting the quality of drinking water due to their high content of dyes and toxic substances, urging the need for finding simple and cost-effective remedies to remove such contaminants. Industrial dyes represent one of the most common classes of chemicals that cause drinking water contamination [1]. Based on their charge in aqueous solutions, dyes can be classified into cationic (basic dyes), anionic (acidic dyes), and non-ionic (dispersed dyes) [2,3]. Dyes are mostly applied in the textile industry because of their bright color, water-solubility, low cost, and feasibility of application to the fabric. Yet, these dyes can be released as environmental pollutants not only during the tanning process but also as part of the waste resulting from household laundry drainage water. Due to their aromatic nature, synthetic dye degradation in the environment may lead to the production of highly toxic products that are resistant to oxidizing agents and heat or biodegradation, rendering them to be hazardous not only to humans but also to aquatic life [4].

MB is one of the common cationic industrial dyes that is highly used in cotton, silk, and paper dyeing [5,6]. It also has some applicability in biomedical and therapeutic fields [7]

and in food production [8,9]. Many human health diseases were found to result from contact with MB, such as mental disorders and blindness [10,11]. The community of biological systems is also affected as a result of a decrease in the transmittance of sunlight due to MB solubility in water due to the change in its color [12,13]. MB is non-biodegradable, carcinogenic, and toxic; this requires an effective, low-cost, fast, and eco-friendly approach for its removal from water. Several methods, such as liquid–liquid extraction [14], nanofiltration [15,16], coagulation [17,18], ultrafiltration [19,20], adsorption/biosorption [21,22], etc., were reported in the literature.

Among previously reported water treatment methods, adsorption-based methods are considered highly efficient, fast, and inexpensive approaches [23]. “Natural solid bio-adsorbents, especially from plant wastes, are considered to be an attractive remedy for water treatment being eco-friendly, low cost, biodegradable, and reliable in terms of green chemistry friendly materials. Their absorption efficiency depends on several parameters, including the surface area of the adsorbent, particle size, and amount, besides some other interaction conditions such as pH, temperature, and contact time with the target samples.

Many examples are reported in literature involving bio-adsorbents for the removal of toxic chemical compounds, heavy metals, and dyes, some of which include wheat and rice [24], remainings of coffee and tea [25,26], leaves and barks of dry trees [27–29], powder of saw and coir [30–32], and shell of rice [33,34] and natural polymers such as chitosan, lignin and in some cases micro-organisms that were reported to be capable of dyes degradation [25,35].

Hydrogels are materials with 10% of their constitutional weight or volume made of water. The existence of hydrophilic groups in the hydrogel network, such as (-NH₂, -COOH, -OH, CONH₂, -CONH, and -SO₃H), is the main reason for their hydrophilicity [36–38]. The hydrogel 3D structure formed by the polymeric building blocks can be tailored by different modifiers to regulate the affinity of hydrogels to various target pollutants and ionic contaminants and enhance their adsorption ability [39].

In this work, poly acrylic acid (PAA) was used as a sorbent hydrogel in the presence of orange peel (OP), a natural waste material, as a modifier to improve the removal of the MB (as a model cationic dye) from the water based on the benefit of the components comprising the cell walls of OP which are mainly hemicellulose (11%), cellulose (22), sugar (23%), and pectin (25%) [40]. These natural polymers present in OP were reported to show good adsorption properties towards cationic chemicals such as MB [41,42]. The optimum adsorption conditions, including OP content, pH, temperature, and initial dye concentration and adsorption kinetics models (pseudo-first and pseudo-second-order) and isotherm models (Langmuir, Freundlich, and Temkin), were investigated.

2. Materials and Methods

2.1. Materials

All chemicals used were of analytical grade and used without further purification. Deionized distilled water was used in preparation of reagents throughout all experiments. Acrylic acid (AA) from Merck Company, Darmstadt, Germany, Ammonium persulfate (APS), ethylene glycol dimethyl acrylate (EGDMA), and boric acid from Alfa Aesar (Kandel, Germany). Nitric acid and sodium Hydroxide from VWR Chemicals (Darmstadt, Germany). Phosphoric acid, sodium nitrate (NaNO₃), Acetic acid, and Methylene blue (MB) (Sigma-Aldrich company (Schnelldorf, Germany). MB Stock solutions were prepared by dissolving different amounts of powdered dye in Britton–Robinson buffer (BR-B) at different pHs.

2.2. Instrumentation

Jenway UV-Visible Spectrophotometer Model 7205 was used for MB initial and final concentration measurements (Jenway Instruments, St Neots, UK). Jenway 3510 Advanced Bench pH Meter (Jenway Instruments, St Neots, UK). Digital orbital shaker, Mini-scale, SSM1, (Stuart, London, UK), was used for shaking the tested samples during the different adsorption stages. An FTIR-Affinity-1, (Shimadzu Corporation, Kyoto, Japan) was used

in the range 400–4000 cm^{-1} . Ultra-high-resolution scanning electron microscope (SEM) (Model: Leo Supra 55, Zeiss Sigma, Oberkochen, Germany) was used for surface morphology; samples were fixed on aluminum stubs and coated with gold before observation. Brunauer–Emmett–Teller (BET) measurements were used to determine the specific surface area, pore size, and volume using surface area analyzer manufacturer by Quantachrome; model of NOVA touch LX2, the sample was degassed at 150 °C for 2 h under a vacuum.

2.3. Preparation of OP Powder

The orange peel used in this study comes from local Egyptian sweet orange fruit (*Citrus sinensis*). The waste orange peels collected from fresh juice shops or household waste were washed with distilled water, then the colored outer layer of peel was removed by a scrapper to avoid any possible color overlap during the adsorption measurements. The remaining white inner layer of orange peel (OP) was cut into small parts, dried in the microwave, then ground and sieved by a 0.045 mm porous stainless-steel sieve. The resulting dried biomass was stored in a plastic cup until use without any further chemical treatment.

2.4. Adsorbent Hydrogel Preparation

In order to prepare OP-PAA adsorbent hydrogel, as given in Table 1, different amounts of OP were added to deionized DW in 30 mL screw bottle and sonicated for 10 min, followed by stirring for another 10 min in an oil bath at 65 °C. After complete dispersion of OP, the AA monomer (different ratios) was added while stirring to mix, followed by EGDMA as a cross linker (different ratios). After complete homogeneity of the mixture, it was purged with nitrogen gas for 10 min to remove any entrapped oxygen; finally, 5 mL DW containing 250 mg APS was added to the mixture as an initiator. The polymerization reaction was allowed to take place for 2 h at 65 °C, and the resulting OP-PAA polymers were left to dry in a vacuum oven at 60 °C and crushed to be ready for further characterization.

Table 1. OP-PAA Adsorbent hydrogel composite component.

Polymer Name	AA (%)	AA (mL)	OP (g)	EGDMA (mL)	DW (mL)
A	10	3.0	1.0	—	22.0
B	20	6.0	1.0	—	19.0
C	30	9.0	1.0	—	16.0
D	20	6.0	0.5	—	19.0
E	20	6.0	2.0	—	19.0
F	20	6.0	—	—	19.0
G	20	6.0	0.5	0.6	18.4
H	20	6.0	0.5	1.2	17.8
I	20	6.0	0.5	1.8	17.2

2.5. Characterization

2.5.1. The Swelling Capacity Percent (SCP)

In order to study OP-PAA swelling behavior, 0.5 g of OP-PAA in a nylon tea bag was added to 50 mL BR-B (pH 4, 7, and 9) at room temperature (RT), followed by orbit shaking at 130 rpm for 3.5 h. The swelled hydrogel was then taken out from the buffer and weighted, then returned to the buffer again at definite time intervals.

The swelling capacity percent (SCP) was calculated according to the following Equation (1)

$$SCP = \frac{W_f - W_i}{W_i} * 100 \quad (1)$$

where W_f is the weight of dried OP-PAA, and W_i is the weight of swelling OP-PAA.

2.5.2. Determine the Point of Zero Charges (pHPZC)

The solid addition method was used to determine the point of zero charges (pHPZC) of the polymer, according to a previous study [43]. Briefly, 25 mg of OP-PAA was added to 25 mL of 0.1 M NaNO₃. The pH of sodium nitrate solution was adjusted prior to the addition of OP-PAA (from 2 to 10) using either NaOH or HNO₃. The solutions were left for 2 days until equilibrium took place, and the pH of each solution was recorded. Δ pH values were calculated and plotted on the x-axis against the pH on the y-axis.

2.5.3. FTIR Spectra, SEM, and BET Characterization

Fourier transform infrared spectra in the range of 4000–400 cm⁻¹ were used to characterize the chemical structures of prepared polymer with and without dye. Furthermore, SEM and BET were used to determine polymer morphology and surface area, respectively.

2.6. Dye Adsorption and Kinetic Studies

Different OP content by weight (0.5, 1.0, and 2.0 g) of OP-PAA was used to study the OP-PAA hydrogel adsorption efficiency where 250 mg OP-PAA was added to 25 mL MB dye solution (100 mg/L BR-B pH 9.0), and the mixture was agitated at 170 rpm. The dye concentration was measured at different time intervals until equilibrium took place during the kinetic studies. The initial and final concentrations of MB were determined by UV–VIS spectrophotometer and using a linear equation ($y = 0.1751x - 0.1145$, $R^2 = 0.9998$) in the range from 1 to 8 mg/L at λ_{\max} 662 nm. The adsorption capacity and removal ratio for the dye can then be determined according to the following Equations (2) and (3):

$$q_e = \frac{(C_i - C_f) * V}{m} \quad (2)$$

$$RR = \frac{C_i - C_f}{C_i} * 100 \quad (3)$$

where q_e (mg/g) is the adsorption capacity, RR is the removal ratio, C_i (mg/L) is the initial dye concentration, and C_f (mg/L) is the final dye concentration. V (L) dye solution volume and m (g) represents the dried adsorbent weight.

2.7. Desorption Studies

The OP-PAA used in adsorption experiment was separated from the remaining dye by centrifugation, then washed by DW to get rid of unabsorbed MB dye. A total of 2.0 g of Separated adsorbent were then added to 25 mL DW at different pH for 1 h at RT.

3. Results and Discussion

3.1. Characterization of OP-PAA Hydrogel

3.1.1. The Swelling Capacity Percent (SCP)

The swelling behavior of a hydrogel adsorbent plays an important role in its adsorption characteristic [44]. Nine hydrogel polymers (A-I) were prepared with different amounts of AA as a monomer, OP, and EGDMA as a cross-linker, as given in Table 1. The swelling capacity percent (SCP) was determined for the prepared polymers to select the best component ratio exhibiting the highest swelling capacity.

Figure 1A shows the effect of AA percent on the swelling capacity at different pH values. It is clear that the increase in AA percent from 10% (polymer A) to 20% (polymer B) led to an increase in SCP. This increase was due to an increase in the content of carboxylic acid groups. On further increase in AA content from 20% (polymer B) to 30% (polymer C) caused a decrease in SCP. This phenomenon can be attributed to the interaction between the OH groups of OP and the COOH group in AA, rendering the polymer more rigid and, in turn, affecting its swelling tendency [45–47].

Figure 1B represents the effect of variation of OP content effect on SCP. The addition of 0.5 g OP (polymer D) causes an increase in SCP due to introducing more ionizable groups such as OH and COOH present in the cellulose and pectin content of OP, respectively. Further increase in OP to 1 or 2 g was found to cause deterioration of SCP; as a result, the viscosity increased due to the high content of OP, which hinders interaction of the adsorbents with MB [48].

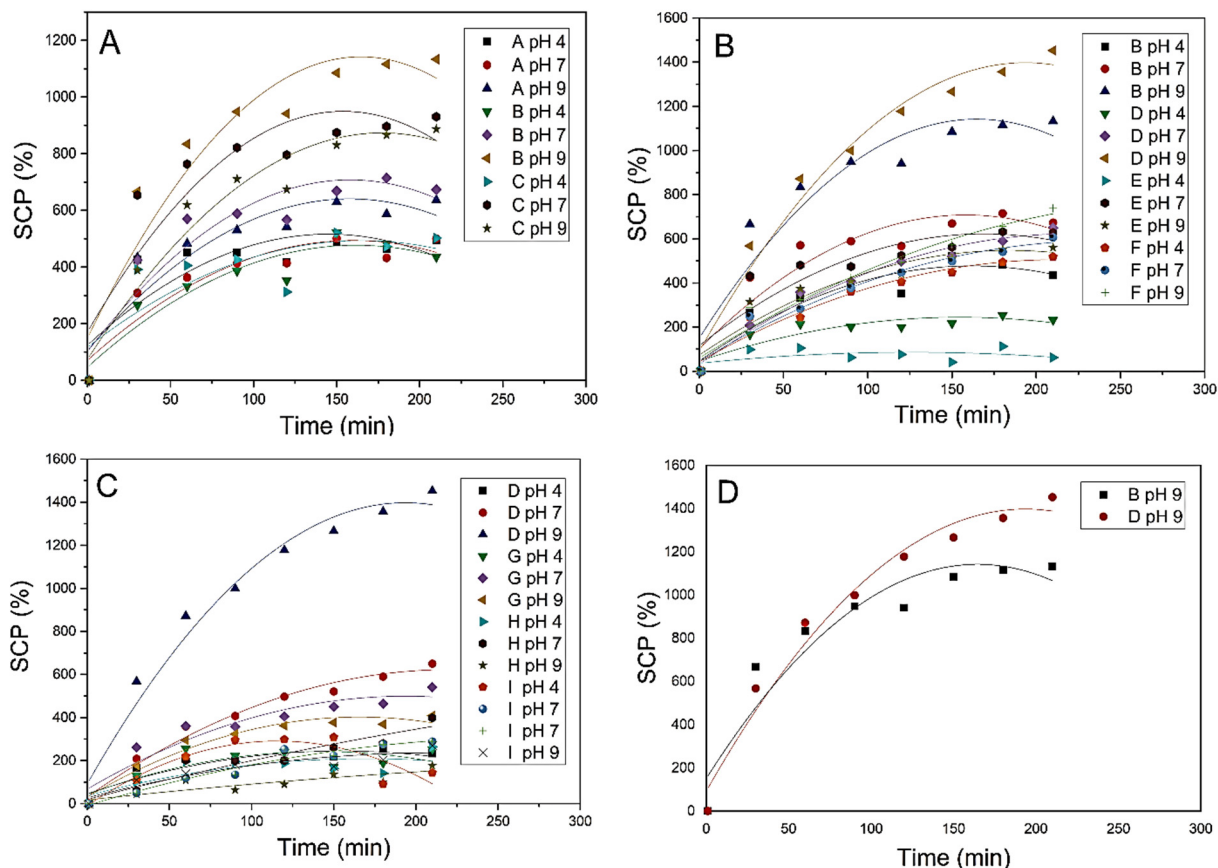


Figure 1. Effect of AA (A), OP (B) and EGDMA percent on SCP (C), and comparison between polymers (B,D) exhibiting the highest absorption efficiency (D).

Finally, the effect of using EGDMA as a cross-linker was studied, as given in Figure 1C. It is clear that the increase in EGDMA concentration was associated with SCP decrease because it renders the water diffusion in the compact hydrogel more difficult. The tendency of SCP to decrease with cross-linker concentration increase was found to be in agreement with the Flory theory and the results of previous studies [49].

The pH effect on SCP was also investigated, and it was found that an increase in SCP was associated with a pH increase. According to the previous result, a hydrogel adsorbent polymer composed of 6 mL AA and 0.5 g OP without using a cross-linker (polymer D) was selected to be used for further adsorption experiments.

3.1.2. Determine the Point of Zero Charges (pHPZC)

pHPZC value plays an important role in the adsorption mechanism understanding where adsorption of cationic dyes such as MB is preferred to take part at pH larger than pHPZC [50]. From the experimental data, it was found that pHPZC values of PAA and poly E are 2.6 and 2.5, respectively, as indicated in Figure 2.

3.1.3. FT-IR Spectra

The FT-IR spectra of PAA, MB, and MB adsorbed on OP-PAA are shown in Figure 3. In PAA FT-IR spectra, a band at 2921 cm^{-1} that refers to the C-H stretching of an alkane is noticed due to complete AA polymerization. Another two bands at 1632 and 1456 cm^{-1} can be assigned to symmetric and asymmetric stretching vibrations of COO^- , respectively. FT-IR spectrum of MB has many bands; the most characteristic are 1638 , 1416 , and 543 cm^{-1} , which correspond to C=N stretching, C-N stretching vibration in aromatic amines, and C-S skeleton vibration, respectively [51,52].

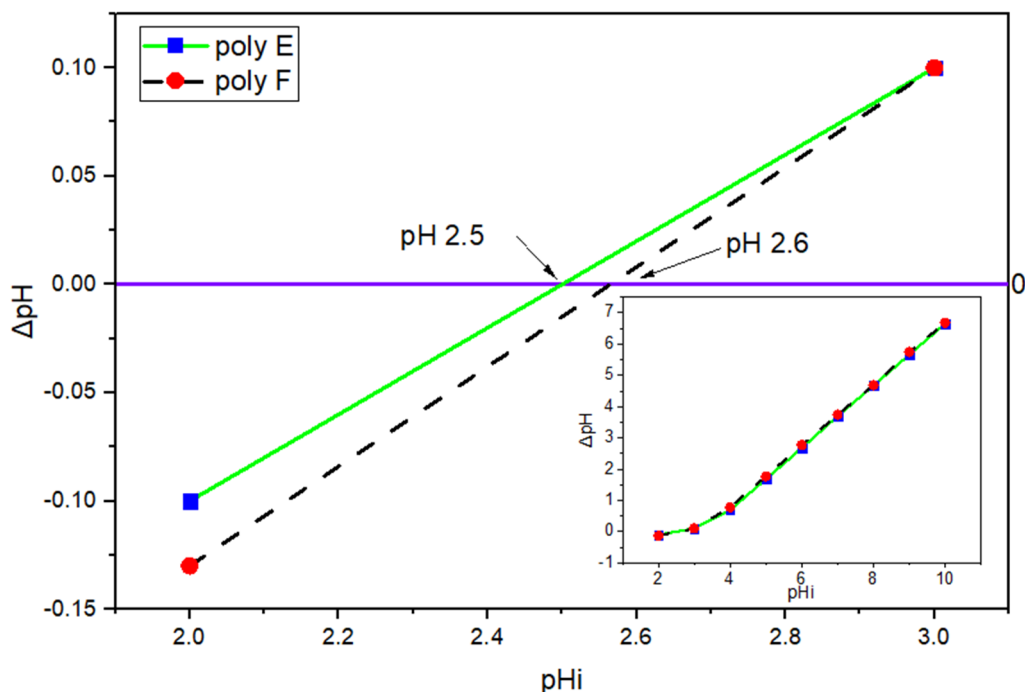


Figure 2. Relation between ΔpH and initial pH and pH_{PZC} conclusion.

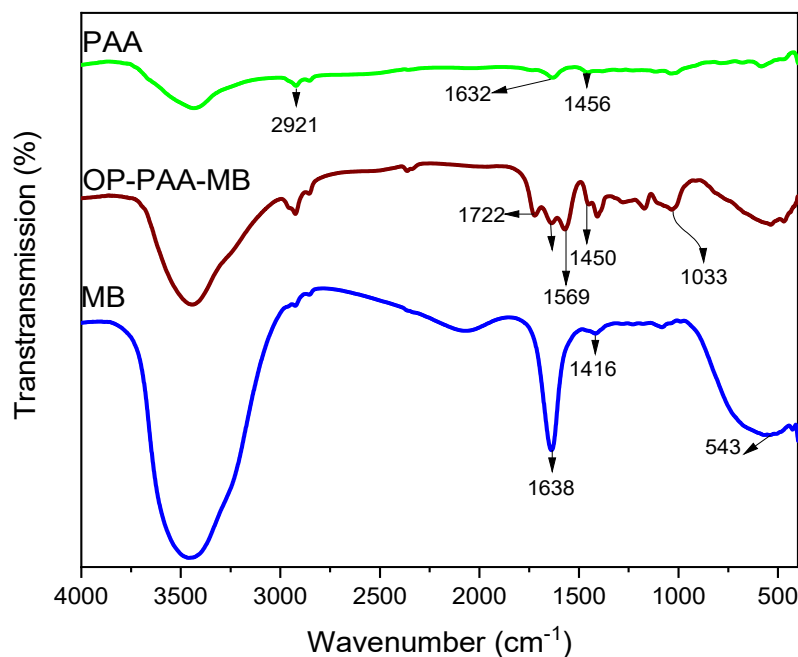


Figure 3. FT-IR spectra of PAA, MB, and MB adsorbed on polymer E hydrogel.

Due to OP's complex nature, a lot of bands were noticed in its FTIR spectrum. The bands 1722 , 1033 , and 1450 cm^{-1} can be associated with C=O stretching, indicating the abundant carboxylic groups that are capable of interaction and binding with MB; also, the band at 1569 cm^{-1} can be assigned to N-O stretching.

The FT-IR spectra of PAA, MB, and MB adsorbed on OP-PAA showed a clear OH band at 3500 cm^{-1} , the reduction in the intensity of the OH band indicated its participation in blending and cross-linking mechanism with the cationic MB dye, which agrees with the previously reported results for orange peel interaction with textile dyes indicating the role of OH groups in adsorption [53,54].

3.1.4. BET

The surface area (SA) of the adsorbent is one of the main influencing parameters affecting its adsorption efficiency. Multipoint Brunaur–Emmett Teller (BET) analysis was used to determine the polymer's SA using N_2 gas adsorption and desorption, as given in Figure 4A. While, Barrett–Joyner–Halenda (BJH) analysis was used to detect the pore volume of polymers F, E, and polymer E after adsorption of MB (E-MB) were found to be 0.090 cc/g , 0.111 cc/g , and 0.025 cc/g , respectively as given in Table 2 and Figure 4B,C. Polymer F was found to show a relatively higher surface area (SA) of $66.5\text{ m}^2/\text{g}$ compared to that of polymer E $53.1\text{ m}^2/\text{g}$ and polymer E-MB $22.9\text{ m}^2/\text{g}$. Although the SA of polymer E is smaller [45] than that of polymer F, the adsorption capacity of polymer E was found to be the largest.

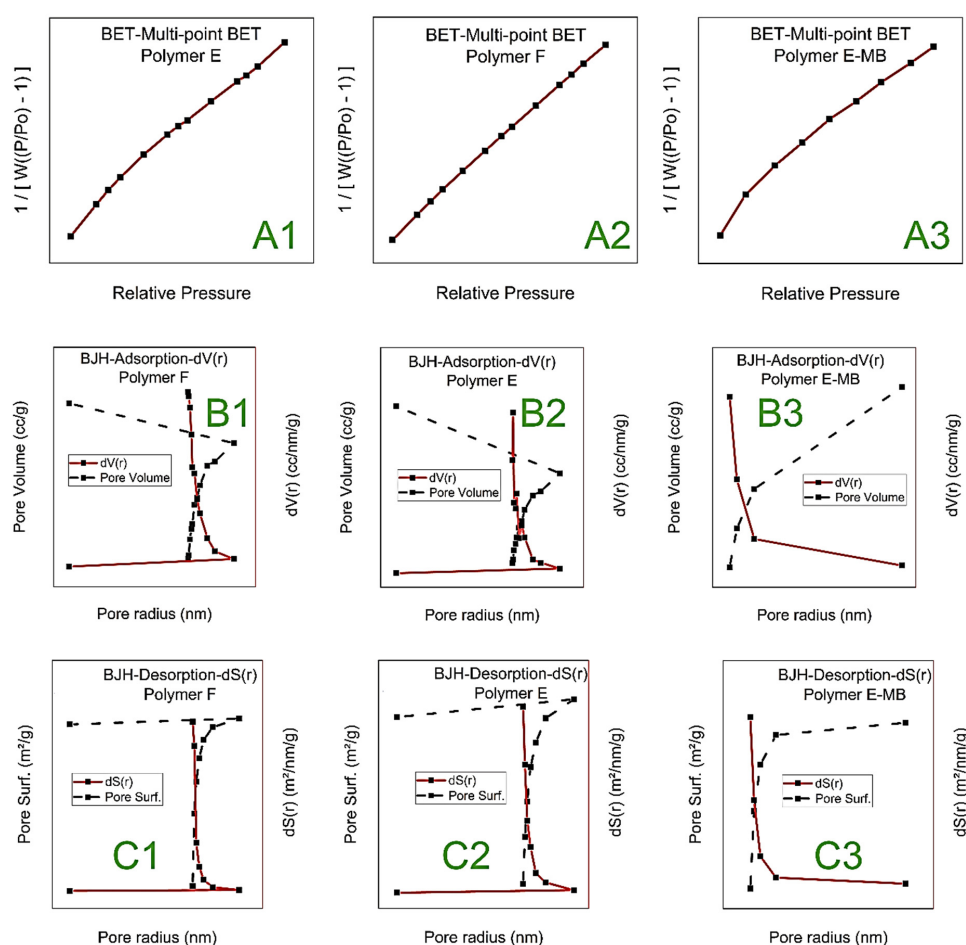


Figure 4. BET-Multi-point BET for polymer F (A1), polymer E (A2), and MB adsorbed on polymer E (A3). BJH Pore Size Distribution-Adsorption for polymer F (B1), polymer E (B2), and MB adsorbed on polymer E (B3). BJH Pore Size Distribution-Desorption for polymer F (C1), polymer E (C2), and MB adsorbed on polymer E (C3).

Table 2. Surface area, pore volume and radius of polymer F, polymer E, and MB adsorbed on polymer E.

	Unit	Polymer F	Polymer E	Polymer E-MB
Surface Area by multipoint BET	mc ² /g	66.51	53.11	22.86
Pore Volume by BJH	cc/g	0.090	0.111	0.025
pore radius by BJH	nm	2.087	1.734	1.684

These phenomena can be correlated to the large pore volume of polymer E and its high content of OH and COOH groups as a result of OP addition. Polymer E-MB has the smallest pore volume and SA due to the adsorption of MB dye on the polymer surface. Furthermore, the pore radius of polymer E was found to decrease from 1.734 nm to 1.684 nm in the presence of MB; this can be attributed to the high adsorbed amount of MB, which indicated the strong interaction between the OP and the PAA polymer [45,46,53].

3.1.5. SEM

Figure 5 shows the surface morphology of polymer F (5A), polymer E (5B), and polymer E after adsorption of MB (E-MB) (5C) at three different magnification power (1, 3, and 7 KX). Polymer F, comprising PAA only, showed a homogenous polymeric nature, as shown in Figure 5A, whereas the addition of OP to PAA, Figure 5B, was found to increase the surface area by increasing the pores and cavities in the polymeric matrix. The change in textural properties and roughness of polymer E after the adsorption of MB, as shown in Figure 5C, represented evidence of the accumulation of MB onto the bio-adsorbent surface.

3.2. Effect of OP Content

The effect of OP content on swelling and hydrogel adsorption capacity is presented in Figure 6. It is clear that upon the addition of 0.5 g OP to PAA, Polymer D, q_e was increased compared to polymer F comprising PAA only. This can be attributed to the introduction of OH and COOH groups from cellulose and pectin, respectively, that represented the main components in OP, where –OH reacts with AA and increases the polymeric network [55,56]. The increase in the swelling capacity also participates in adsorption capacity enhancement due to the increase in the surface area of the adsorbent [44,57,58].

Further increase in the content of OP, though, increases the adsorption capacity and velocity of adsorption, but on the other hand, results in a decrease in the swelling efficiency. This can be explained based on the increase in the number of –OH groups due to the increase in cellulose content, which may act as a cross-linker upon reaction with AA monomer increasing the polymer rigidity. However –COOH groups on the pectin surface are capable of maintaining the adsorption capacity value stable and increasing the rate of adsorption. According to OP content results, polymer E, comprising 6 mL AA and 2.0 g OP, was selected as hydrogel adsorbent to complete the next adsorption experiments as it showed the highest adsorption capacity among the prepared hydrogels.

3.3. Effect of pH

The variation of pH of the medium plays an important role in protonation and deprotonation not only of the MB but the hydrogel adsorbent itself due to its enriched content of carboxylic and hydroxyl groups; thus, the effect of pH on adsorption of MB (100 mg/L) at RT was investigated. In order to discuss the pH effect of MB adsorption, the pH_{PZC} must be determined where cationic dye adsorption is preferred at a pH higher than pH_{PZC} [39,50], as given in Figure 7. From experimental data, pH_{PZC} values of PAA and polymer E were found to be 2.6 and 2.5, respectively.

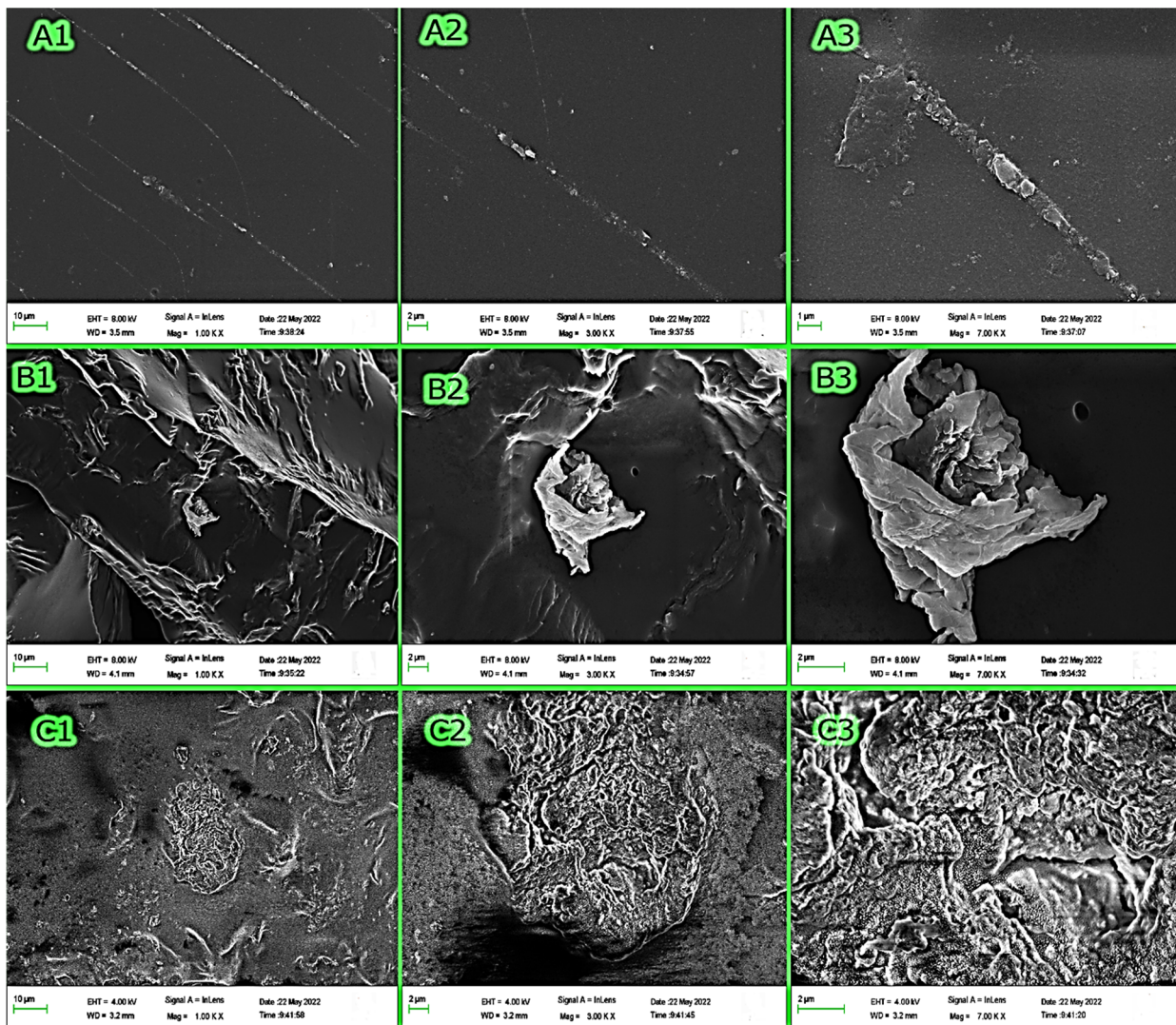


Figure 5. SEM images of polymer F (A), Polymer E (B), and MB adsorbed on polymer E (C).

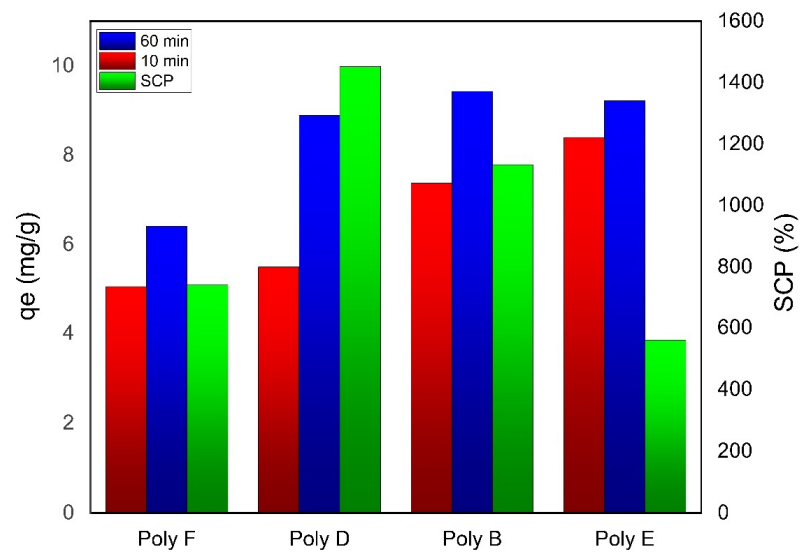


Figure 6. Effect of OP content on q_e of both PAA and OP-PAA for MB adsorption. Experimental conditions were: MB concentration 100 mg/L; adsorbent hydrogel dose 250 mg in 25 mL; pH 9 at RT.

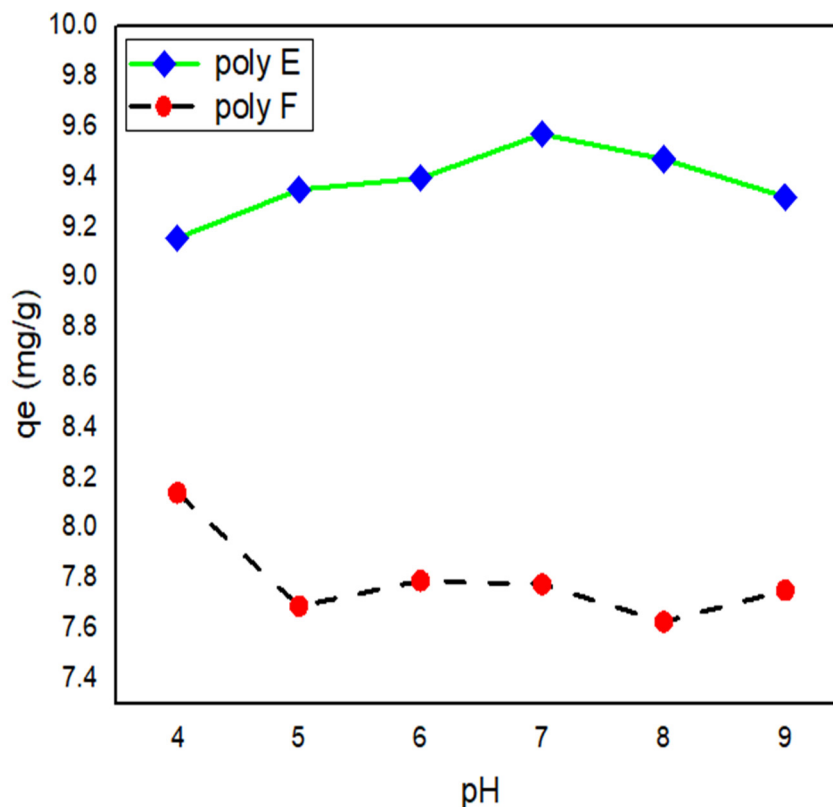


Figure 7. Effect of pH on q_e of both polymer F and polymer E for MB adsorption. Experimental conditions were: MB concentration: 100 mg/L; h adsorbents hydrogel dose: 250 mg in 25 mL and RT.

The variation in q_e was found to be relatively small at low pH and peaks at pH 7.0. This can be attributed to the protonation of $-\text{COOH}$ at low pH, where $-\text{H}$ from HCl is bound to the carboxylic group in acrylate. As the pH increases, COOH becomes deprotonated and more COO^- groups are generated and are available for reaction with MB [59]. On the other hand, the increase in pH value results in an increase in the swelling ratio paired with increased polymer surface area and more MB penetration. At pH higher than 7.0, the q_e was found to decrease due to the charge screening effect of sodium ions and competition between sodium ions from NaOH and MB to interact with the carboxylate groups of the polymer [60,61].

3.4. Effect of Temperature

The effect of temperature on adsorption is an important factor to be investigated in order to have an insight into the adsorption thermodynamics parameters such as entropy ΔS , enthalpy ΔH , and free energy ΔG . MB adsorption on PAA and OP-PAA adsorbent hydrogel was found to decrease with a temperature increase from 30 to 60 °C, as shown in Figure 8. Although the increase in temperature commonly causes swelling of internal adsorbent construction and, in turn, increases the dye molecules penetration [62], it also causes dye ions' mobility to increase. This increase in ion mobility is associated with an adsorption capacity decrease, which agrees with the behavior previously reported [63,64].

The change in entropy ΔS , enthalpy ΔH , and free energy ΔG was calculated by using Equations (4)–(7) [65,66]:

$$K_d = \frac{[A(s)]}{[A(l)]} = \frac{q_e}{C_e} \quad (4)$$

$$\Delta G = -RT \ln K_d \quad (5)$$

$$\Delta G = \Delta H - T\Delta S \quad (6)$$

$$\ln(K_d) = \frac{\Delta S}{R} - \frac{\Delta H}{RT} \quad (7)$$

where C_f and C_i are the final and initial MB concentrations (mg/L), K_d , R , and T are the equilibrium constant, the gas constant, and temperature (K), respectively.

Figure 8 represents the Van't Hoff plot where $\ln K_d$ was plotted against $1/T$. ΔS and ΔH can be calculated from the Van't Hoff plot using the intercept and slope. Table 3 shows the thermodynamic values; by increasing Temperature, ΔG values move to be a positive value, which means that the MB adsorption process on the hydrogel adsorbent is spontaneous [67,68]. ΔH and ΔS values are negative, as commonly associated with exothermic processes, indicating a randomness decrease at the solid/liquid interface [69,70].

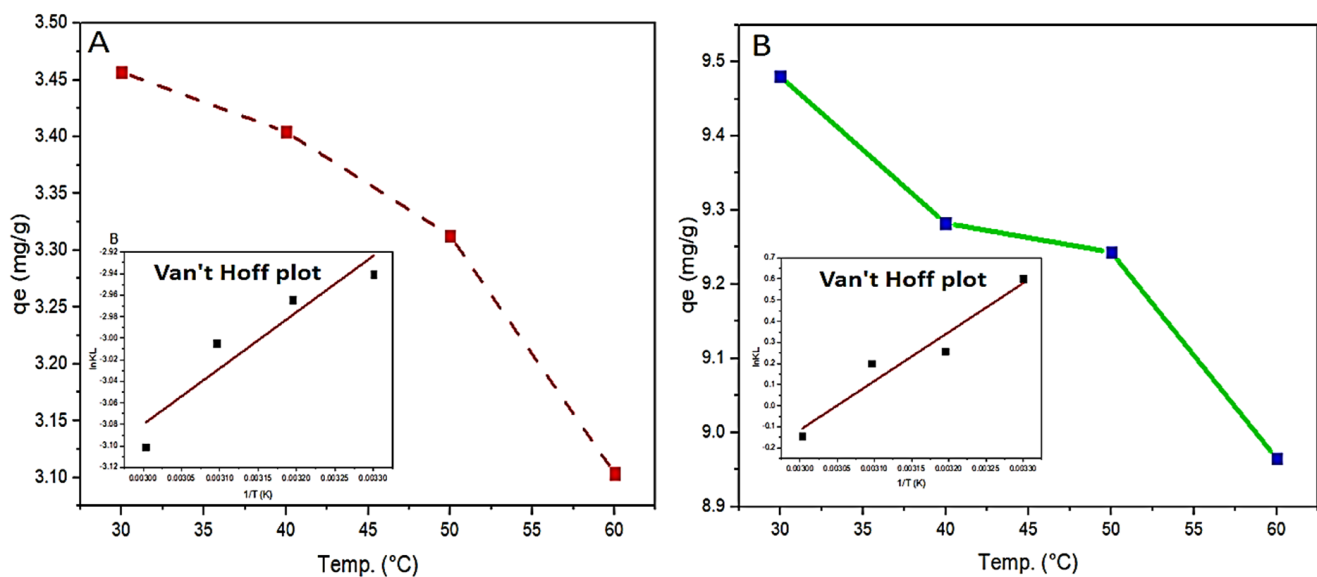


Figure 8. Effect of temperature and Van't Hoff plot on q_e of polymer F (A) and polymer E (B) for MB adsorption. Experimental conditions were: MB concentration: 100 mg/L; adsorbents hydrogel dose 250 mg in 25 mL; pH 7.

Table 3. Polymers E and F thermodynamic parameters for MB adsorption.

	Temperature	Polymer E	Polymer F
ΔG (KJmol ⁻¹)	30 °C	−1.52	7.41
	40 °C	−0.67	7.71
	50 °C	−0.54	8.07
	60 °C	0.40	8.59
ΔH (KJmol ⁻¹)		−19.23	−4.34
ΔS (KJ ⁻¹ mol ⁻¹)		−58.64	−38.62

3.5. Adsorption Kinetics

In order to investigate the adsorption kinetics of OP-PAA and MB, the time effect on adsorption capacities was studied. Figure 9 shows the relationship between time (min) and polymer E and F adsorption capacities at a definite time (min) and q_t (mg/g). It can be noticed that, at the first 10 min, a rapid adsorption rate took place where about 84% of MB was adsorbed by OP-PAA. Then, the rate of adsorption became slow until equilibrium took place at 60 min with a removal ratio, RR, of about 92%). This can be attributed to the presence of a large, uncovered absorbent surface area at the beginning of the experiment, which decreased over time upon the start of MB adsorption and accumulation of the adsorbent surface. On further increase in time for another hour, the RR value was found to reach 94% and remained stable thereafter when tested up to 5 h.

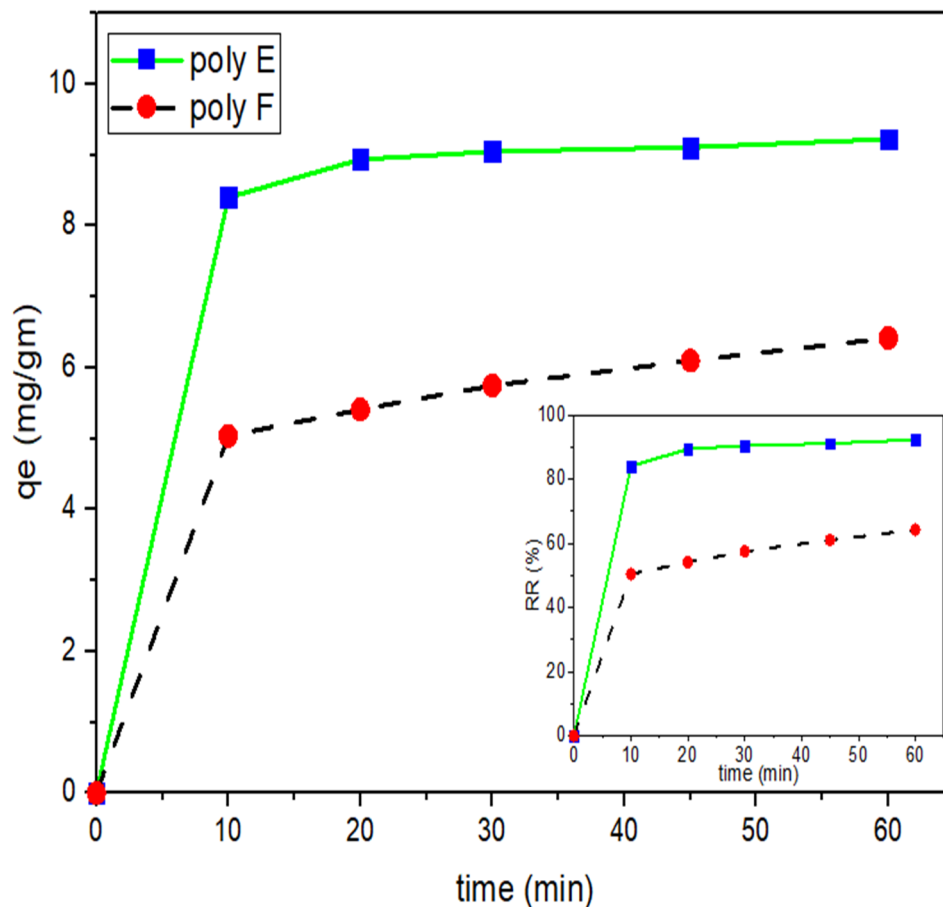


Figure 9. Effect of contact time on q_t of both PAA and OP-PAA for MB adsorption. Experimental conditions were: MB concentration 100 mg/L; adsorbents hydrogel dose 250 mg in 25 mL; pH 9 at RT.

On the other hand, on comparing with unmodified PAA as an adsorbent, RR values were found to be 50% and 64% at 10 and 60 min, respectively, with no further increase. Accordingly, it can be concluded that the addition of OP to PAA enhances the removal ratio from 50% to 84% in the first ten min and increases the RR rate to 92% after one hr.

The adsorption kinetics were tested using both pseudo-first and pseudo-second-order models [71].

The pseudo-first-order linear Equation (8) can be represented as [59]:

$$\log(q_e - q_t) = \log q_e - \frac{K_1 t}{2.303} \tag{8}$$

while the pseudo-second-order linear Equation (9) can be indicated by [72]:

$$\frac{t}{q_t} = \frac{1}{K_2 q_e^2} + \frac{t}{q_e} \tag{9}$$

where q_t (mg/g) and q_e are the adsorption capacities at a definite time (min) and equilibrium, respectively, K_1 (1/min) and K_2 (g/mg min⁻¹) are the rate constants of adsorption for pseudo-first- and second-order, respectively.

The experimental data were used to plot $\log(q_e - q_t)$ and t/q_t against t , as shown in Figure 10, in order to calculate K_1 and K_2 , and q_e from the intercept and slope of the plots as given in Table 4.

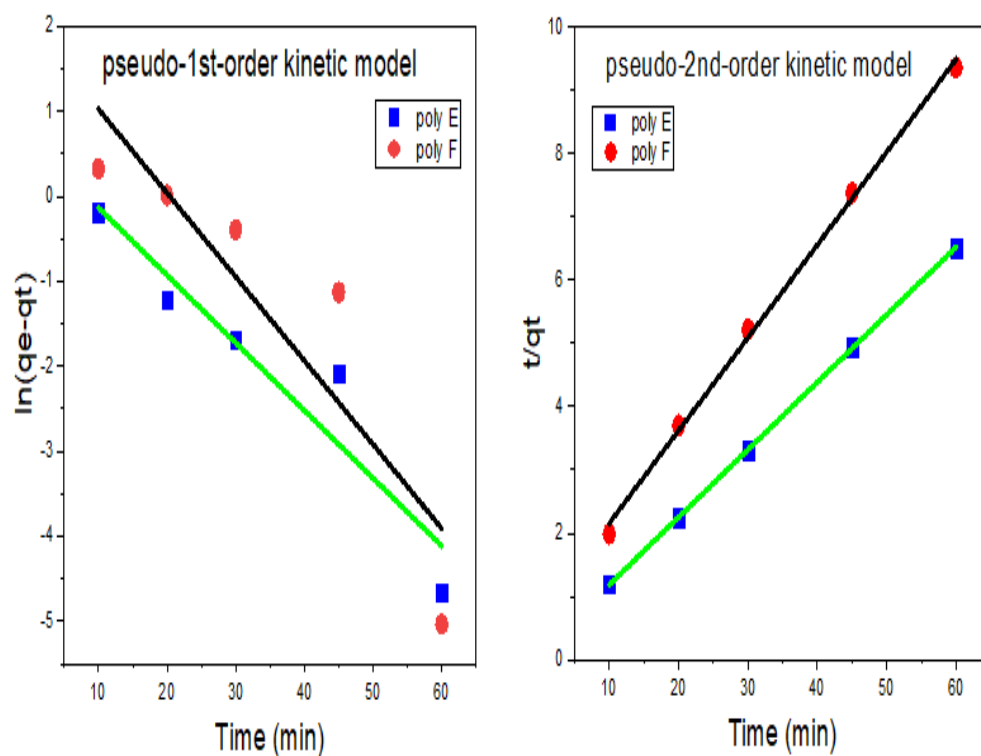


Figure 10. Kinetics curves of pseudo-first-order and pseudo-second-order model. Experimental conditions were, MB concentration 100 mg/L; adsorbents hydrogel dose 250 mg in 25 mL; pH 9; RT.

Table 4. Polymer E and F kinetic parameters for MB adsorption.

Parameters	Pseudo-First-Order				Pseudo-Second-Order			
	K_1 min^{-1}	Cal q_e mg/g	Exp q_e mg/g	R_1^2	K_2 $\text{mg}^{-1} \text{min}^{-1}$	Cal q_e mg/g	Exp q_e mg/g	R_2^2
Polymer E	−0.0013275	1.9	9.2	0.8692	0.09582068	9.4	9.2	0.9999
Polymer F	−0.0016448	7.5	6.4	0.7384	0.03129885	6.8	6.4	0.9969

R^2 of the pseudo-first-order model was found to be 0.739 and 0.869 for PAA and OP-PAA, respectively, while the calculated q_e were 7.5 and 1.9 mg/g for PAA and OP-PAA, respectively. The previous result indicated that the pseudo-first-order model does not fit with experimental data. In contrast, R^2 for the pseudo-second-order model was found to be 0.9969 and 0.9999 for PAA and OP-PAA, respectively, indicating better fitting to such a model. Besides the R^2 value being highly close to 1.0, the calculated q_e was close enough to the experimental q_e ; thus, based on the data shown in Table 4, it can be concluded that the pseudo-second-order model is suitable to describe the adsorption of MB onto OP-PAA hydrogel.

3.6. Adsorption Isotherms

The correlation between the initial concentration of MB (C_i) and the equilibrium absorption capacity, q_e , was studied, as shown in Figure 11. It was found that the increase in C_i from 200 to 1800 mg/L led to a dramatic increase in q_e from 135 to 1309 mg/g for polymer F and from 317 to 1933 mg/g for polymer E. From this result, it can be concluded that the addition of OP to PAA improves the adsorption efficiency of the adsorbent hydrogel.

Langmuir, Freundlich, and Temkin isotherm models were used to test the interaction mechanism between MB and adsorbent hydrogel.

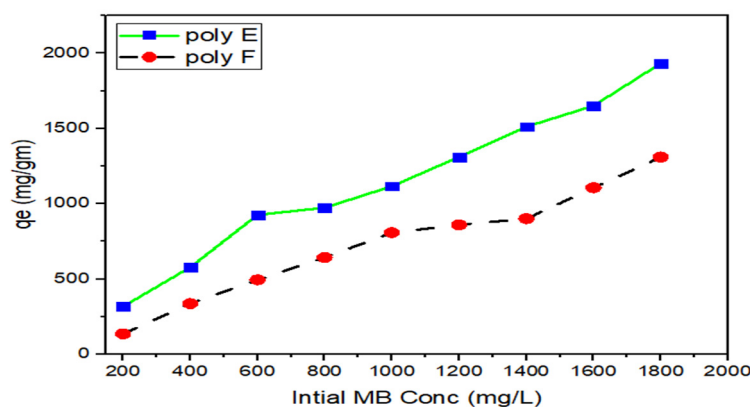


Figure 11. Effect of initial MB concentration on both polymer F and polymer E for MB adsorption. Experimental conditions were: adsorbents hydrogel dose 50 mg in 100 mL; pH 7, and RT.

The Langmuir linear Equation (10) form is [73]:

$$\frac{1}{q_e} = \frac{1}{q_m} + \frac{1}{q_m K_L C_e} \quad (10)$$

The Freundlich linear Equation (11) form is [74]:

$$\log q_e = \log K_f + \frac{1}{n} \log C_e \quad (11)$$

The Temkin linear Equation (12) form is [23]:

$$q_e = \frac{RT}{b} \ln(K_T C_e) \quad (12)$$

where q_m (mg/g) and q_e represent the maximum and equilibrium adsorption capacities, respectively. C_i (mg/L) is the initial dye concentration, while K_L (L mg⁻¹), K_F (mg^{1-1/n} L^{1/n} g⁻¹), and K_T Lg⁻¹ are the isotherm constants of Langmuir, Freundlich, and Temkin, respectively.

Figure 12 and Table 5 show the fitting curves of the tested isotherm models and their parameters. The highest R^2 value for polymer E was found to be related to the Langmuir isotherm model (0.964) with a calculated q_m close enough to the experimental q_e . Freundlich and Temkin's models showed R^2 of 0.932 and 0.873, respectively. This indicated that the adsorption of MB on polymer E could be better described by Langmuir rather than Freundlich and Temkin models.

On the other hand, R^2 of Langmuir and Freundlich for polymer F were equal (0.95) with negative sign q_m when calculated using Langmuir models, which indicated that MB adsorption on polymer F follows Freundlich rather than Langmuir's model. Furthermore, the Temkin model showed a good R^2 value (0.929) and can be used to describe the adsorption of MB on polymer F.

3.7. Desorption of MB

In order to study the regeneration and reusability of the OP-PAA, the polymers bound to MB were separated by centrifugation, then washed by DW to get rid of any unadsorbed MB dye. A total of 2.0 g of the separated adsorbent were incubated in 25 mL DW of different pH values for 1 h at RT. Desorption studies play a role in understanding the adsorption mechanism.

It is noteworthy to mention that if the MB adsorbed on the hydrogel adsorbent can be removed by DW, this means that the attraction between MB and hydrogel adsorbent is very weak. On the other hand, if the attraction between MB and hydrogel adsorbent can be destroyed by an acid such as HCl, this indicates that the mechanism can be correlated more to electrostatic attraction or ion exchange [50].

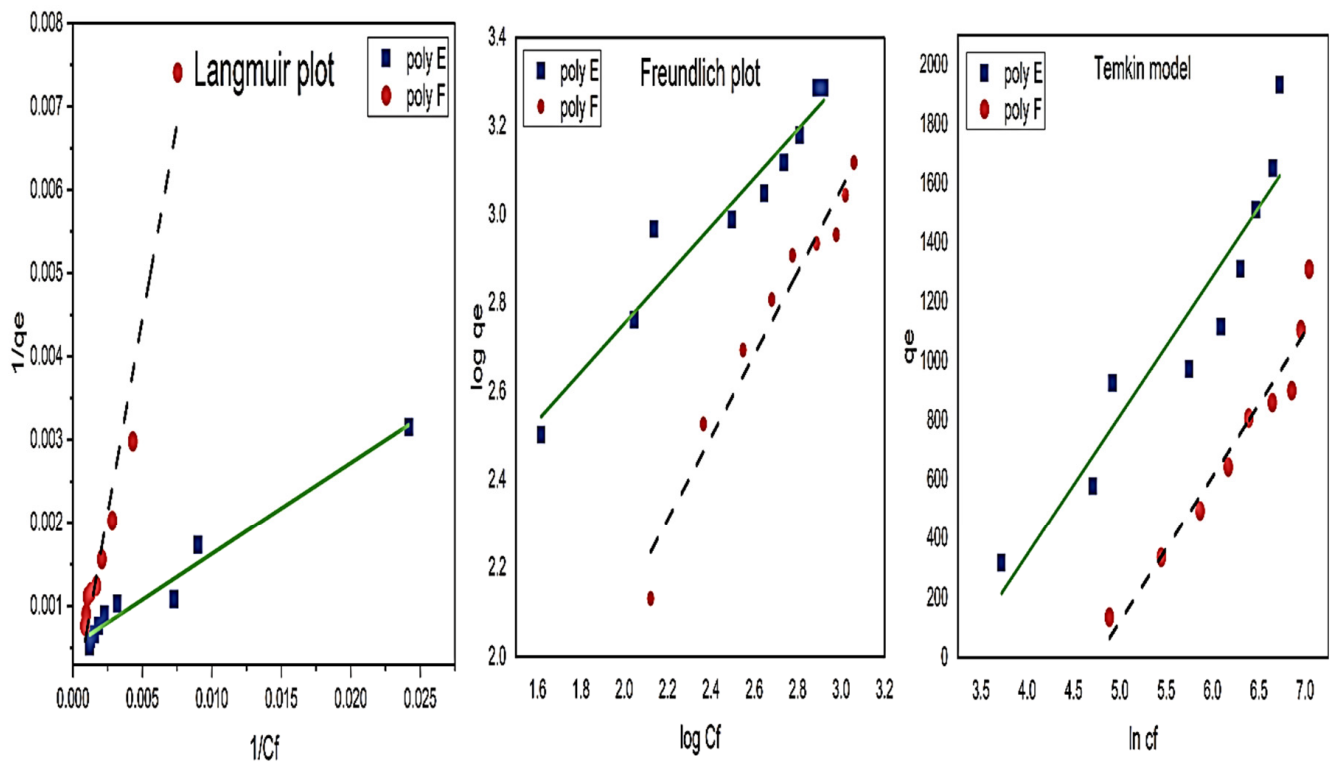


Figure 12. Isotherm model plots of both polymer F and E for MB adsorption. Experimental conditions were: adsorbents hydrogel dose 50 mg in 100 mL; pH 7, at RT.

Table 5. Polymers E and F isotherm parameters for MB adsorption at 25 °C.

	Parameters	Unit	Polymer E	Polymer F
Langmuir model	q_m	mg/g	1892	−4379
	K_L	L/mg	0.00482	−0.00024
	R^2		0.964	0.953
Freundlich model	$1/n$		0.5485	0.9357
	K_f		45.3	1.78
	R^2		0.932	0.950
Temkin model	B_T	J/mol	469	489
	K_T	L/gm	0.0383	0.0086
	R^2		0.873	0.929

The experimental results showed the occurrence of no desorption of MB from the hydrogel adsorbent at pH ranging from three to nine, while efficient removal of MB was attained at pH 2, as represented in Figure 13. Desorption at pH 2 can be correlated to the low value of pH_{PZC} of the hydrogel adsorbent and indicated that the MB was attached to the hydrogel adsorbent via electrostatic attraction rather than surface adsorption.

The desorbed OP-PAA hydrogel reusability was tested, and it was found to retain its efficiency in terms of absorption capacity without any change for not less than ten times of usage and desorption, which indicated the usability of the hydrogel polymer after simple treatment with HCl.



Figure 13. Adsorption and Desorption of MB from Polymer E at different pH (2–9). Experimental conditions were: adsorbents hydrogel dose: 2.0 g in 25 mL for 1 h at RT.

4. Conclusions

In this work, a simple approach for the removal of cationic dye based on the combination of poly acrylic acid (PAA) as a sorbent hydrogel in the presence of Orange peel (OP) as a natural modifier to improve the removal of the MB (as a model cationic dye) is reported. MB adsorption by OP-PAA and PAA was found to be affected by the amount of OP, initial pH value, reaction temperature, and initial dye concentration. The addition of OP to PAA was found to enhance the adsorption capacity of PAA and accelerate the adsorption process. q_e of both polymer E and F adsorbent hydrogels were optimized at pH 7, and RT temperature increases were found to have a negative effect on q_e . The max adsorption capacity of polymer E was calculated by the Langmuir isotherm to be equal to 1892 mg/g.

Comparison of the adsorption parameters of OP-PAA hydrogel adsorbent, presented in this work and other previously reported dyes' adsorbents given in Table 6 [75–82], indicated that the presented adsorbent is not only an inexpensive and cost-effective, green and recyclable but was found to be more effective and fast acting for dye removal, where 84% of the adsorption was attained in 10 min without any need for stirring. The desorption process of MB, as a model cationic molecule, from OP-PAA hydrogel adsorbent was found to efficiently take place at pH 2.0 indicating that MB interaction with the hydrogel adsorbent took place via electrostatic attraction rather than surface adsorption which indicates the efficient ability of the hydrogel to retain the adsorbed dye particles. Furthermore, the prepared OP-PAA adsorbent hydrogel was found to be regenerable using HCl at pH 2 and retained its efficiency after several adsorption/desorption cycles, which indicated that the presented OP-PAA adsorbent hydrogel is a promising cost-effective, and efficient, reusable eco-friendly adsorbent for water treatment, from cationic moieties that can either be dyes or heavy metal ions.

Table 6. Comparison between OP-PAA and some other previously reported dyes' adsorbents.

Adsorbent	Dye	q _m mg/g	RR%	Time	Ref
Tragacanth gum and carboxyl-functionalized carbon nanotube	Methylene blue	1092	80.0	40 min	[75]
Sludge	Direct red 28	1.25	—	100 min	[76]
<i>Haloxylon recurvum</i> stem	Acid brown 354	6.87	81.0	50 min	[77]
Coconut Shell (Activated carbon)	Crystal violet	44.00	99.6	24 h	[78]
Orange peel	Methylene blue	—	95.7	24 h	[54]
Spent tea leave	Methylene blue	—	99.0	24 h	[54]
Rattan sawdust	Methylene blue	359.00	—	480 min	[79]
Acacia nilotica sawdust	Methylene blue	46.95	99.9	60 min	[80]
Starch-g-poly (acrylic acid)	Methylene blue	1532	—	30 min	[81]
Gum ghatti-g-poly(acrylic acid)	Methylene blue	909	99	75 min	[82]
Orange peel poly (Acrylic acid)	Methylene blue	1892	84.0	10 min	This work

Author Contributions: Conceptualization, S.R.A.-M. and R.M.E.N.; methodology, S.R.A.-M., N.A.-H.A.-T. and R.M.E.N.; validation, N.A.-H.A.-T.; investigation, N.A.-H.A.-T.; resources, S.R.A.-M. and R.M.E.N.; writing—original draft preparation, N.A.-H.A.-T.; writing—review and editing, S.R.A.-M. and N.A.-H.A.-T.; R.M.E.N. supervision, R.M.E.N. All authors have read and agreed to the published version of the manuscript.

Funding: This research received no external funding.

Institutional Review Board Statement: Not applicable.

Informed Consent Statement: Not applicable.

Data Availability Statement: All data will be available upon reasonable request from the corresponding author.

Conflicts of Interest: The authors declare no conflict of interest.

References

- Khan, I.; Saeed, K.; Zekker, I.; Zhang, B.; Hendi, A.H.; Ahmad, A.; Ahmad, S.; Zada, N.; Ahmad, H.; Shah, L.A.; et al. Eeview on methylene blue: Its properties, uses, toxicity and photodegradation. *Water* **2022**, *14*, 242. [CrossRef]
- Thomas, B.; Shilpa, E.P.; Alexander, L.K. Role of functional groups and morphology on the pH-dependent adsorption of a cationic dye using banana peel, orange peel, and neem leaf bio-adsorbents. *Emergent Mater.* **2021**, *4*, 1479–1487. [CrossRef]
- Nirmaladevi, S.; Palanisamy, N. A comparative study of the removal of cationic and anionic dye from aqueous solutions using biochar as an adsorbent. *Desalin. Water Treat.* **2020**, *175*, 282–292. [CrossRef]
- Pirkarami, A.; Olya, M.E.; Yousefi Limaee, N. Decolorization of azo dyes by photo electro adsorption process using polyaniline coated electrode. *Prog. Org. Coat.* **2013**, *76*, 682–688. [CrossRef]
- Derakhshan, Z.; Baghapour, M.A.; Ranjbar, M.; Faramarzian, M. Adsorption of methylene blue dye from aqueous solutions by modified pumice stone: Kinetics and equilibrium studies. *Health Scope* **2013**, *2*, 136–144. [CrossRef]
- Han, T.H.; Khan, M.M.; Kalathil, S.; Lee, J.; Cho, M.H. Simultaneous enhancement of methylene blue degradation and power generation in a microbial fuel cell by gold nanoparticles. *Ind. Eng. Chem. Res.* **2013**, *52*, 8174–8181. [CrossRef]
- Dao, H.M.; Whang, C.H.; Shankar, V.K.; Wang, Y.H.; Khan, I.A.; Walker, L.A.; Husain, I.; Khan, S.I.; Murthy, S.N.; Jo, S. Methylene blue as a far-red light-mediated photocleavable multifunctional ligand. *Chem. Commun.* **2020**, *56*, 1673–1676. [CrossRef]
- Koyuncu, H.; Kul, A.R. Removal of methylene blue dye from aqueous solution by nonliving lichen (*Pseudevernia furfuracea* (L.) Zopf.), as a novel biosorbent. *Appl. Water Sci.* **2020**, *10*, 72. [CrossRef]
- Balarak, D.; Bazzi, M.; Shehu, Z.; Chandrika, K. Application of surfactant-modified bentonite for methylene blue adsorption from aqueous solution. *Orient. J. Chem.* **2020**, *36*, 293–299. [CrossRef]
- Santoso, E.; Ediati, R.; Kusumawati, Y.; Bahruji, H.; Sulistiono, D.O.; Prasetyoko, D. Review on recent advances of carbon based adsorbent for methylene blue removal from waste water. *Mater. Today Chem.* **2020**, *16*, 100233. [CrossRef]

11. Abdelrahman, E.A.; Hegazey, R.M.; El-Azabawy, R.E. Efficient removal of methylene blue dye from aqueous media using Fe/Si, Cr/Si, Ni/Si, and Zn/Si amorphous novel adsorbents. *J. Mater. Res. Technol.* **2019**, *8*, 5301–5313. [[CrossRef](#)]
12. Zhou, S.; Du, Z.; Li, X.; Zhang, Y.; He, Y.; Zhang, Y. Degradation of methylene blue by natural manganese oxides: Kinetics and transformation products. *R. Soc. Open Sci.* **2019**, *6*, 190351. [[CrossRef](#)]
13. Kosswattaarachchi, A.M.; Cook, T.R. Repurposing the industrial dye methylene blue as an active component for redox flow batteries. *ChemElectroChem* **2018**, *5*, 3437–3442. [[CrossRef](#)]
14. El-Ashtouky, E.S.Z.; Fouad, Y.O. Liquid-liquid extraction of methylene blue dye from aqueous solutions using sodium dodecylbenzenesulfonate as an extractant. *Alex. Eng. J.* **2015**, *54*, 77–81. [[CrossRef](#)]
15. Kong, G.; Pang, J.; Tang, Y.; Fan, L.; Sun, H.; Wang, R.; Feng, S.; Feng, Y.; Fan, W.; Kang, W.; et al. Efficient dye nanofiltration of a graphene oxide membrane: Via combination with a covalent organic framework by hot pressing. *J. Mater. Chem. A* **2019**, *7*, 24301–24310. [[CrossRef](#)]
16. Zhong, F.; Wang, P.; He, Y.; Chen, C.; Li, H.; Yu, H.; Chen, J. Preparation of stable and superior flux GO/LDH/PDA-based nanofiltration membranes through electrostatic self-assembly for dye purification. *Polym. Adv. Technol.* **2019**, *30*, 1644–1655. [[CrossRef](#)]
17. Lau, Y.Y.; Wong, Y.S.; Teng, T.T.; Morad, N.; Rafatullah, M.; Ong, S.A. Degradation of cationic and anionic dyes in coagulation-flocculation process using bi-functionalized silica hybrid with aluminum-ferric as auxiliary agent. *RSC Adv.* **2015**, *5*, 34206–34215. [[CrossRef](#)]
18. Liu, J.; Li, P.; Xiao, H.; Zhang, Y.; Shi, X.; Lü, X.; Chen, X. Understanding flocculation mechanism of graphene oxide for organic dyes from water: Experimental and molecular dynamics simulation. *AIPL Adv.* **2015**, *5*, 117151. [[CrossRef](#)]
19. Zheng, L.; Su, Y.; Wang, L.; Jiang, Z. Adsorption and recovery of methylene blue from aqueous solution through ultrafiltration technique. *Sep. Purif. Technol.* **2009**, *68*, 244–249. [[CrossRef](#)]
20. Kim, S.; Yu, M.; Yoon, Y. Fouling and retention mechanisms of selected cationic and anionic dyes in a Ti₃C₂T_x MXene-ultrafiltration hybrid system. *ACS Appl. Mater. Interfaces* **2020**, *12*, 16557–16565. [[CrossRef](#)]
21. Wang, Z.; Gao, M.; Li, X.; Ning, J.; Zhou, Z.; Li, G. Efficient adsorption of methylene blue from aqueous solution by graphene oxide modified persimmon tannins. *Mater. Sci. Eng. C* **2020**, *108*, 110196. [[CrossRef](#)] [[PubMed](#)]
22. Li, H.; Liu, L.; Cui, J.; Cui, J.; Wang, F.; Zhang, F. High-efficiency adsorption and regeneration of methylene blue and aniline onto activated carbon from waste edible fungus residue and its possible mechanism. *RSC Adv.* **2020**, *10*, 14262–14273. [[CrossRef](#)] [[PubMed](#)]
23. Madrakian, T.; Afkhami, A.; Ahmadi, M. Adsorption and kinetic studies of seven different organic dyes onto magnetite nanoparticles loaded tea waste and removal of them from wastewater samples. *Spectrochim. Acta Part A Mol. Biomol. Spectrosc.* **2012**, *99*, 102–109. [[CrossRef](#)]
24. Juang, R.S.; Ju, C.Y. Equilibrium sorption of copper(II)-ethylenediaminetetraacetic acid chelates onto cross-linked, polyaminated chitosan beads. *Ind. Eng. Chem. Res.* **1997**, *36*, 5403–5409. [[CrossRef](#)]
25. Chang, M.Y.; Juang, R.S. Adsorption of tannic acid, humic acid, and dyes from water using the composite of chitosan and activated clay. *J. Colloid Interface Sci.* **2004**, *278*, 18–25. [[CrossRef](#)] [[PubMed](#)]
26. Vieira, R.S.; Beppu, M.M. Interaction of natural and crosslinked chitosan membranes with Hg(II) ions. *Colloids Surf. A Physicochem. Eng. Asp.* **2006**, *279*, 196–207. [[CrossRef](#)]
27. Tsai, W.T.; Chang, C.Y.; Lin, M.C.; Chien, S.F.; Sun, H.F.; Hsieh, M.F. Adsorption of acid dye onto activated carbons prepared from agricultural waste bagasse by ZnCl₂ activation. *Chemosphere* **2001**, *45*, 51–58. [[CrossRef](#)]
28. Mall, I.D.; Srivastava, V.C.; Agarwal, N.K.; Mishra, I.M. Removal of congo red from aqueous solution by bagasse fly ash and activated carbon: Kinetic study and equilibrium isotherm analyses. *Chemosphere* **2005**, *61*, 492–501. [[CrossRef](#)]
29. Mitchell, M.; Ernst, W.R.; Lightsey, G.R.; Rasmussen, E.T.; Bagherzadeh, P. Adsorption of textile dyes by activated carbon produced from agricultural, municipal and industrial wastes. *Bull. Environ. Contam. Toxicol.* **1978**, *19*, 307–311. [[CrossRef](#)]
30. Ghosh, D.; Bhattacharyya, K.G. Adsorption of methylene blue on kaolinite. *Appl. Clay Sci.* **2002**, *20*, 295–300. [[CrossRef](#)]
31. Muthukumar, M.; Selvakumar, N. Studies on the effect of inorganic salts on decolouration of acid dye effluents by ozonation. *Dye. Pigment.* **2004**, *62*, 221–228. [[CrossRef](#)]
32. Alinsafi, A.; Khemis, M.; Pons, M.N.; Leclerc, J.P.; Yaacoubi, A.; Benhammou, A.; Nejmeddine, A. Electro-coagulation of reactive textile dyes and textile wastewater. *Chem. Eng. Process. Process Intensif.* **2005**, *44*, 461–470. [[CrossRef](#)]
33. Han, R.; Ding, D.; Xu, Y.; Zou, W.; Wang, Y.; Li, Y.; Zou, L. Use of rice husk for the adsorption of congo red from aqueous solution in column mode. *Bioresour. Technol.* **2008**, *99*, 2938–2946. [[CrossRef](#)]
34. Chakraborty, S.; Chowdhury, S.; Das Saha, P. Adsorption of crystal violet from aqueous solution onto NaOH-modified rice husk. *Carbohydr. Polym.* **2011**, *86*, 1533–1541. [[CrossRef](#)]
35. Staroń, P.; Chwastowski, J. Raphia-Microorganism Composite Biosorbent for Lead Ion Removal from Aqueous Solutions. *Materials* **2021**, *14*, 7482. [[CrossRef](#)]
36. Bekiari, V.; Sotiropoulou, M.; Bokias, G.; Lianos, P. Use of poly(N,N-dimethylacrylamide-co-sodium acrylate) hydrogel to extract cationic dyes and metals from water. *Colloids Surf. A Physicochem. Eng. Asp.* **2008**, *312*, 214–218. [[CrossRef](#)]
37. Yetimoğlu, E.K.; Kahraman, M.V.; Ercan, Ö.; Akdemir, Z.S.; Apohan, N.K. N-vinylpyrrolidone/acrylic acid/2-acrylamido-2-methylpropane sulfonic acid based hydrogels: Synthesis, characterization and their application in the removal of heavy metals. *React. Funct. Polym.* **2007**, *67*, 451–460. [[CrossRef](#)]

38. El Mansoub, A.; El Sayed, M.M.; El Nashar, R.M.; Fahmy, H.M.; Abulnour, A.M.G. Chemically/Electrically-Assisted Regeneration of Polyacrylonitrile-based Hydrogel adsorbed Heavy Metals. *Egypt. J. Chem.* **2022**, *65*, 373–384. [[CrossRef](#)]
39. Wang, L.; Zhang, J.; Wang, A. Fast removal of methylene blue from aqueous solution by adsorption onto chitosan-g-poly (acrylic acid)/attapulgitite composite. *Desalination* **2011**, *266*, 33–39. [[CrossRef](#)]
40. Ayala, J.R.; Montero, G.; Coronado, M.A.; García, C.; Curiel-Alvarez, M.A.; León, J.A.; Sagaste, C.A.; Montes, D.G. Characterization of orange peel waste and valorization to obtain reducing sugars. *Molecules* **2021**, *26*, 1348. [[CrossRef](#)]
41. Sun, G.; Xu, X. Sunflower stalks as adsorbents for color removal from textile wastewater. *Ind. Eng. Chem. Res.* **1997**, *36*, 808–812. [[CrossRef](#)]
42. Panneerselvam, P.; Morad, N.; Tan, K.A. Magnetic nanoparticle (F3O4) impregnated onto tea waste for the removal of nickel(II) from aqueous solution. *J. Hazard. Mater.* **2011**, *186*, 160–168. [[CrossRef](#)] [[PubMed](#)]
43. Balistrieri, L.S.; Murray, J.W. The surface chemistry of goethite (alpha -FeOOH) in major ion seawater. *Am. J. Sci.* **1981**, *281*, 788–806. [[CrossRef](#)]
44. Tally, M.; Atassi, Y. Synthesis and characterization of pH-sensitive superabsorbent hydrogels based on sodium alginate-g-poly(acrylic acid-co-acrylamide) obtained via an anionic surfactant micelle templating under microwave irradiation. *Polym. Bull.* **2016**, *73*, 3183–3208. [[CrossRef](#)]
45. Pavithra, S.; Thandapani, G.; Sugashini, S.; Sudha, P.N.; Alkhamis, H.H.; Alrefaei, A.F.; Almutairi, M.H. Batch adsorption studies on surface tailored chitosan/orange peel hydrogel composite for the removal of Cr (VI) and Cu (II) ions from synthetic wastewater. *Chemosphere* **2021**, *271*, 129415. [[CrossRef](#)]
46. Yati, I.; Kizil, S.; Bulbul Sonmez, H. Cellulose-based hydrogels for water treatment. In *Cellulose-Based Superabsorbent Hydrogels*; Springer: Berlin/Heidelberg, Germany, 2019; pp. 1015–1037.
47. Shankar, P.; Thandapani, G.; Kumar, V.; Parappurath Narayanan, S. Evaluation of batch and packed bed adsorption column for chromium (VI) ion removal from aqueous solution using chitosan-silica-g-AM/orange peel hydrogel composite. *Biomass Convers. Biorefinery* **2022**, 1–16. [[CrossRef](#)]
48. Kowalski, G.; Kijowska, K.; Witczak, M.; Kuterasiński, L.; Lukaszewicz, M. Synthesis and effect of structure on swelling properties of hydrogels based on high methylated pectin and acrylic polymers. *Polymers* **2019**, *11*, 114. [[CrossRef](#)]
49. Flory, P.J.; Rehner, J. Statistical mechanics of cross-linked polymer networks I. rubberlike elasticity. *J. Chem. Phys.* **1943**, *11*, 512–520. [[CrossRef](#)]
50. Mall, I.D.; Srivastava, V.C.; Kumar, G.V.A.; Mishra, I.M. Characterization and utilization of mesoporous fertilizer plant waste carbon for adsorptive removal of dyes from aqueous solution. *Colloids Surf. A Physicochem. Eng. Asp.* **2006**, *278*, 175–187. [[CrossRef](#)]
51. Fernando, M.S.; de Silva, R.M.; de Silva, K.M.N. Synthesis, characterization, and application of nano hydroxyapatite and nanocomposite of hydroxyapatite with granular activated carbon for the removal of Pb²⁺ from aqueous solutions. *Appl. Surf. Sci.* **2015**, *351*, 95–103. [[CrossRef](#)]
52. Xie, Z.; Guan, W.; Ji, F.; Song, Z.; Zhao, Y. Production of Biologically Activated Carbon from Orange Peel and Landfill Leachate Subsequent Treatment Technology. *J. Chem.* **2014**, *2014*, 491912. [[CrossRef](#)]
53. Kallem, P.; Ouda, M.; Bharath, G.; Hasan, S.W.; Banat, F. Enhanced water permeability and fouling resistance properties of ultrafiltration membranes incorporated with hydroxyapatite decorated orange-peel-derived activated carbon nanocomposites. *Chemosphere* **2022**, *286*, 131799. [[CrossRef](#)] [[PubMed](#)]
54. Lazim, Z.M.; Mazuin, E.; Hadibarata, T.; Yusop, Z. The removal of methylene blue and remazol brilliant blue r dyes by using orange peel and spent tea leaves. *J. Teknol.* **2015**, *74*. [[CrossRef](#)]
55. Li, A.; Wang, A. Synthesis and properties of clay-based superabsorbent composite. *Eur. Polym. J.* **2005**, *41*, 1630–1637. [[CrossRef](#)]
56. Li, A.; Wang, A.; Chen, J. Studies on poly(acrylic acid)/attapulgitite superabsorbent composite. I. synthesis and characterization. *J. Appl. Polym. Sci.* **2004**, *92*, 1596–1603. [[CrossRef](#)]
57. Wang, M.; Li, X.; Zhang, T.; Deng, L.; Li, P.; Wang, X.; Hsiao, B.S. Eco-friendly poly(acrylic acid)-sodium alginate nanofibrous hydrogel: A multifunctional platform for superior removal of Cu(II) and sustainable catalytic applications. *Colloids Surf. A Physicochem. Eng. Asp.* **2018**, *558*, 228–241. [[CrossRef](#)]
58. Toledo, P.V.O.; Limeira, D.P.C.; Siqueira, N.C.; Petri, D.F.S. Carboxymethyl cellulose/poly(acrylic acid) interpenetrating polymer network hydrogels as multifunctional adsorbents. *Cellulose* **2019**, *26*, 597–615. [[CrossRef](#)]
59. Paulino, A.T.; Guilherme, M.R.; Reis, A.V.; Campese, G.M.; Muniz, E.C.; Nozaki, J. Removal of methylene blue dye from an aqueous media using superabsorbent hydrogel supported on modified polysaccharide. *J. Colloid Interface Sci.* **2006**, *301*, 55–62. [[CrossRef](#)]
60. Dai, H.; Huang, H. Enhanced swelling and responsive properties of pineapple peel arboxymethyl cellulose-g-poly(acrylic acid-co-acrylamide) superabsorbent hydrogel by the introduction of carclazyte. *J. Agric. Food Chem.* **2017**, *65*, 565–574. [[CrossRef](#)]
61. Bello, K.; Sarojini, B.K.; Narayana, B.; Rao, A.; Byrappa, K. A study on adsorption behavior of newly synthesized banana pseudo-stem derived superabsorbent hydrogels for cationic and anionic dye removal from effluents. *Carbohydr. Polym.* **2018**, *181*, 605–615. [[CrossRef](#)]
62. Bhattacharyya, K.G.; Sarma, A. Adsorption characteristics of the dye, brilliant green, on neem leaf powder. *Dye. Pigment.* **2003**, *57*, 211–222. [[CrossRef](#)]

63. Wang, L.; Zhang, J.; Wang, A. Removal of methylene blue from aqueous solution using chitosan-g-poly(acrylic acid)/montmorillonite superadsorbent nanocomposite. *Colloids Surf. A Physicochem. Eng. Asp.* **2008**, *322*, 47–53. [[CrossRef](#)]
64. Lv, Q.; Hu, X.; Zhang, X.; Huang, L.; Liu, Z.; Sun, G. Highly efficient removal of trace metal ions by using poly(acrylic acid) hydrogel adsorbent. *Mater. Des.* **2019**, *181*, 107934. [[CrossRef](#)]
65. Chen, T.; Da, T.; Ma, Y. Reasonable calculation of the thermodynamic parameters from adsorption equilibrium constant. *J. Mol. Liq.* **2021**, *322*, 114980. [[CrossRef](#)]
66. Yuan, Z.; Wang, J.; Wang, Y.; Liu, Q.; Zhong, Y.; Wang, Y.; Li, L.; Lincoln, S.F.; Guo, X. Preparation of a poly(acrylic acid) based hydrogel with fast adsorption rate and high adsorption capacity for the removal of cationic dyes. *RSC Adv.* **2019**, *9*, 21075–21085. [[CrossRef](#)]
67. Ramos-Jacques, A.L.; Lujan-Montelongo, J.A.; Silva-Cuevas, C.; Cortez-Valadez, M.; Estevez, M.; Hernandez-Martínez, A.R. Lead (II) removal by poly(N,N-dimethylacrylamide-co-2-hydroxyethyl methacrylate). *Eur. Polym. J.* **2018**, *101*, 262–272. [[CrossRef](#)]
68. Raju, M.P.; Raju, K.M. Design and synthesis of superabsorbent polymers. *J. Appl. Polym. Sci.* **2001**, *80*, 2635–2639. [[CrossRef](#)]
69. Dai, J.; Yan, H.; Yang, H.; Cheng, R. Simple method for preparation of chitosan/poly(acrylic acid) blending hydrogel beads and adsorption of copper(II) from aqueous solutions. *Chem. Eng. J.* **2010**, *165*, 240–249. [[CrossRef](#)]
70. Wang, X.; Zheng, Y.; Wang, A. Fast removal of copper ions from aqueous solution by chitosan-g-poly(acrylic acid)/attapulgitite composites. *J. Hazard. Mater.* **2009**, *168*, 970–977. [[CrossRef](#)]
71. Azizian, S. Kinetic models of sorption: A theoretical analysis. *J. Colloid Interface Sci.* **2004**, *276*, 47–52. [[CrossRef](#)]
72. Ho, Y.S.; McKay, G. Pseudo-second order model for sorption processes. *Process Biochem.* **1999**, *34*, 451–465. [[CrossRef](#)]
73. Osmari, T.A.; Gallon, R.; Schwaab, M.; Barbosa-Coutinho, E.; Severo, J.B.; Pinto, J.C. Statistical analysis of linear and non-linear regression for the estimation of adsorption isotherm parameters. *Adsorpt. Sci. Technol.* **2013**, *31*, 433–458. [[CrossRef](#)]
74. Freundlich, H.; Heller, W. The Adsorption of cis- and trans-Azobenzene. *J. Am. Chem. Soc.* **1939**, *61*, 2228–2230. [[CrossRef](#)]
75. Mallakpour, S.; Tabesh, F. Green and plant-based adsorbent from tragacanth gum and carboxyl-functionalized carbon nanotube hydrogel bionanocomposite for the super removal of methylene blue dye. *Int. J. Biol. Macromol.* **2021**, *166*, 722–729. [[CrossRef](#)] [[PubMed](#)]
76. Aragaw, T.A. Utilizations of electro-coagulated sludge from wastewater treatment plant data as an adsorbent for direct red 28 dye removal. *Data Br.* **2020**, *28*, 104848. [[CrossRef](#)] [[PubMed](#)]
77. Hassan, W.; Noureen, S.; Mustaqeem, M.; Saleh, T.A.; Zafar, S. Efficient adsorbent derived from Haloxylon recurvum plant for the adsorption of acid brown dye: Kinetics, isotherm and thermodynamic optimization. *Surf. Interfaces* **2020**, *20*, 100510. [[CrossRef](#)]
78. Aljeboree, A.M.; Alkaim, A.F. Role of plant wastes as an ecofriendly for pollutants (crystal violet dye) removal from aqueous solutions. *Plant Arch.* **2019**, *19*, 902–905.
79. Islam, M.A.; Ahmed, M.J.; Khanday, W.A.; Asif, M.; Hameed, B.H. Mesoporous activated carbon prepared from NaOH activation of rattan (*Lacosperma secundiflorum*) hydrochar for methylene blue removal. *Ecotoxicol. Environ. Saf.* **2017**, *138*, 279–285. [[CrossRef](#)]
80. Lataye, D.H. Removal of crystal violet and methylene blue dyes using Acacia nilotica sawdust activated carbon. *Indian J. Chem. Technol.* **2019**, *26*, 52–68.
81. Liu, X.; Wei, Q. Removal of methylene blue from aqueous solution using porous starch-g-poly(acrylic acid) superadsorbents. *RSC Adv.* **2016**, *6*, 79853–79858. [[CrossRef](#)]
82. Fosso-Kankeu, E.; Mittal, H.; Mishra, S.B.; Mishra, A.K. Gum ghatti and acrylic acid based biodegradable hydrogels for the effective adsorption of cationic dyes. *J. Ind. Eng. Chem.* **2015**, *22*, 171–178. [[CrossRef](#)]

Disclaimer/Publisher’s Note: The statements, opinions and data contained in all publications are solely those of the individual author(s) and contributor(s) and not of MDPI and/or the editor(s). MDPI and/or the editor(s) disclaim responsibility for any injury to people or property resulting from any ideas, methods, instructions or products referred to in the content.